

Helical Self-Organization and Hierarchical Self-Assembly of an Oligoheterocyclic Pyridine – Pyridazine Strand into Extended Supramolecular Fibers

Louis A. Cuccia,^[a, b] Eliseo Ruiz,^[a, c] Jean-Marie Lehn,^{*, [a]} Jean-Claude Homo,^[d] and Marc Schmutz^[d]

Abstract: The synthesis and characterization of an alternating pyridine – pyridazine strand comprising thirteen heterocycles are described. Spontaneous folding into a helical secondary structure is based on a general molecular self-organization process enforced by the conformational information encoded within the primary structure of the molecular strand itself. Conformational control based on heterocyclic “*helicity codons*” illustrates a strategy for designing folding properties into synthetic oligomers (*foldamers*). Strong intermolecular interactions of the highly ordered lock-washer subunits of compound **3** results in hierarchical supramolecular self-assembly into protofibrils and fibrils. Compound **3** also forms mechanically stable two-dimensional Langmuir – Blodgett and cast thin films.

Keywords: density functional calculations • foldamers • helical structures • heterocycles • self-assembly • supramolecular chemistry • thin films

Introduction

A molecular strand may undergo self-organization into a given architecture determined by the structural and conformational features of its constituting units. In particular, it may adopt various geometries resulting in the generation of specific folded structures.^[1, 2] Natural examples include proteins and RNA, and recently, a number of synthetic bioinspired foldamers have been synthesized and studied.^[1–4] Fundamental goals of such investigations are, on one hand, to gain understanding of and control over the generation of specific folding features of molecular strands in general and in particular of biological ones,^[5] as well as, on the other hand, to

prepare novel abiotic or bioinspired materials with new and improved properties related to well-defined folding patterns.

Helicity is an essential structural motif in the three major classes of biological macromolecules: nucleic acids, polypeptides, and polysaccharides, and the majority of synthetic entities investigated are those adopting a helical secondary structure. Several types of helix-forming heterocycle-containing molecular strands have been designed in our group; they include: oligoheterocyclic pyridine – pyrimidine,^[6–11] pyridine – pyridazine,^[12] and pyridine – naphthyridine^[13] sequences, oligoheterocyclic pyridine – pyrimidine hydrazones,^[14] and oligopyridine – dicarboxamides.^[15–17] Other examples of non-peptide aromatic oligomers that form well-defined secondary structures include hydrogen-bonding oligoanthranilamides^[18–20] and strands based on 2,4-dialkoxy-5-aminobenzoic acid,^[21, 22] oligoureas that adopt intramolecularly hydrogen bonded ring conformations,^[23] phenylacetylenes that form dynamic helices due to solvophobic interactions,^[24] and recently proposed hydrogen-bonded naphthyridinylurea oligomers.^[25] The propensity of oligoheterocyclic pyridine – pyrimidine **2** and pyridine – pyridazine **3** sequences to form a helical motif stems from structure-inducing codons that enforce helical winding due to the strongly favored *transoid* conformation^[26] of the α, α' interheterocyclic bonds.^[6, 8–13] The diameter of these helices depends on the heterocycles used and their connectivity. A convention for describing polypeptide helices involves specifying the number of residues per turn followed by a subscript indicating the number of atoms necessary to close the hydrogen bonding (e.g. an α -helix is denoted as a 3.6₁₃-helix).^[27] Helical heterocyclic foldamers can

[a] Prof. Dr. J.-M. Lehn, Dr. L. A. Cuccia, Dr. Eliseo Ruiz

Laboratoire de Chimie Supramoléculaire
ISIS, Université Louis Pasteur
4, rue Blaise Pascal, 67000 Strasbourg (France)
Fax: (+33) 3 88 41 10 20
E-mail: lehn@chimie.u-strasbg.fr

[b] Dr. L. A. Cuccia

Current address: Department of Chemistry & Biochemistry
Concordia University
1455 De Maisonneuve Blvd. Ouest
Montréal, PQ, H3G 1M8 (Canada)

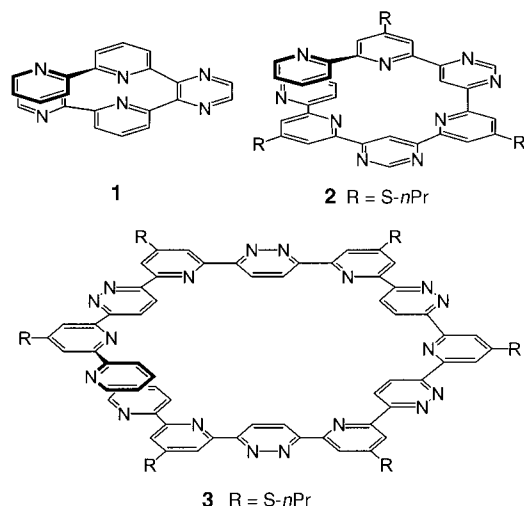
[c] Dr. E. Ruiz

Departament de Química Inorgànica
and Centre Especial de Recerca en Química Teòrica
Universitat de Barcelona
Diagonal 647, 08028 Barcelona (Spain)

[d] Dr. J.-C. Homo, Dr. M. Schmutz

Institut Charles Sadron, CNRS
6, rue Boussingault, 67083 Strasbourg Cedex (France)

be described similarly by specifying the number of heterocycles per turn and the number of atoms required to form a macrocycle. Thus, compound **1**,^[28] with four heterocycles per helix turn and ten atoms required to form a macrocycle is a 4_{10} -helix, compound **2** is a 6_{18} -helix, and compound **3** is a 12_{42} -helix.

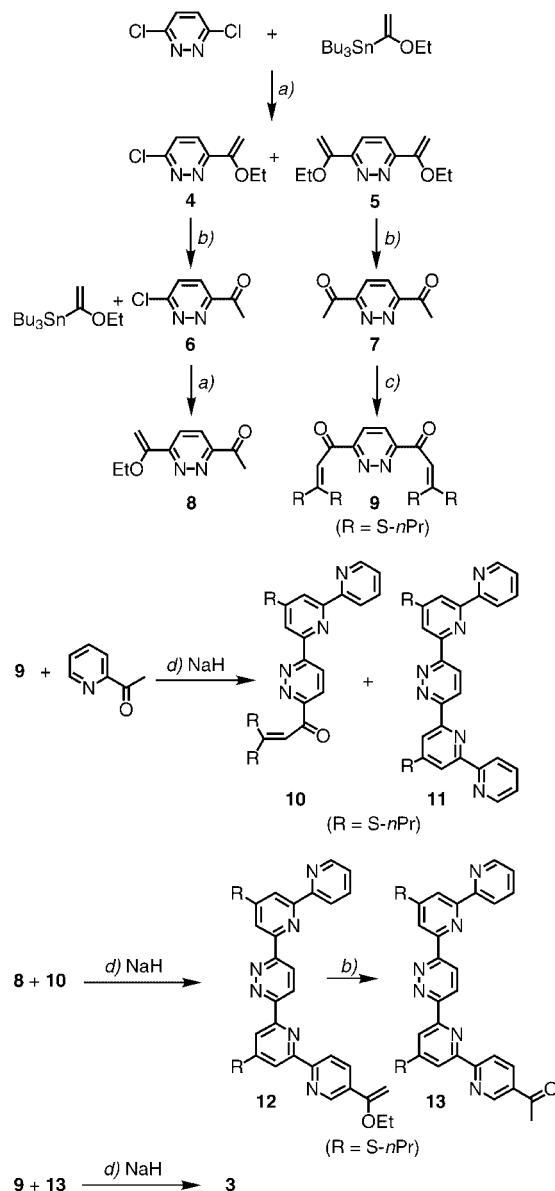


We describe here the synthesis and characterization of an alternating pyridine–pyridazine strand **3** that folds into a helical form presenting twelve heterocycles per turn, an outside diameter of about 25 Å, and a central cavity of about 8 Å across. The molecular framework investigated allows complete control of the final secondary structure. Furthermore, this system also exemplifies the concept of structural hierarchy so prevalent in natural systems. In this particular case, a consequence of the highly ordered helical secondary structure of **3** is that it undergoes further, hierarchical self-assembly into stacked helical filaments, protofibrils, and fibrils in dichloromethane and pyridine.^[12] A model for such stepwise self-assembly of chiral rodlike molecules into tapes, ribbons, fibrils, and fibers has been presented recently.^[29]

Abstract in French: La synthèse et la caractérisation d'un "brin" alterné de pyridine-pyridazine composé de treize hétérocycles sont décrites. La mise en forme spontanée d'une structure secondaire hélicoïdale est basée sur un processus général d'auto-organisation moléculaire induit par l'information conformationnelle codée dans la structure primaire de la molécule elle-même. Cette auto-organisation repose sur des codons d'hélicité hétérocycliques, et illustre une nouvelle stratégie pour programmer les propriétés structurales d'oligomères synthétiques. La géométrie du composé **3** est une hélice et les interactions intermoléculaires entre ces unités hélicoïdales favorisent leur auto-assemblage supramoléculaire, permettant la formation hiérarchique de protofibrilles et fibrilles. Le composé **3** forme également des films bidimensionnels de Langmuir-Blodgett et des couches minces mécaniquement stables.

Results and Discussion

Synthesis of compound 3. Compound **3** was synthesized by using the Potts methodology^[30] along the sequence of reactions shown in Scheme 1. 3-Chloro-6-(1-ethoxy-vinyl)-pyridazine (**4**) and 3,6-bis-(1-ethoxyvinyl)pyridazine (**5**) were



Scheme 1. Reaction sequence for the synthesis of compound **3**. a) $[\text{Pd}(\text{PPh}_3)_2\text{Cl}_2]$, DMF, 80 °C; b) acetone/2N HCl, room temperature; c) NaH, CS_2 , *n*PrI, DMSO, room temperature; d) 1) NaH, THF/DMSO, room temperature; 2) AcOH/ NH_4OAc , reflux.

obtained from 3,6-dichloropyridazine by palladium(II) catalyzed cross-coupling with one or two equivalents of tributyl-(1-ethoxyvinyl)tin in 54 and 58 % yields, respectively. Hydrolysis of **4** and **5** in aqueous acid yielded 3-chloro-6-acetylpyridazine (**6**) and 3,6-diacetylpyridazine (**7**) in 79 and 77 % yields, respectively. The reaction of **6** with tributyl-(1-ethoxyvinyl)tin gave the unsymmetrical product, 3-acetyl-6-(1-ethoxyvinyl)pyridazine (**8**), in 83 % yield. The bis-Michael

acceptor, **9**, was prepared in 66% yield from the sequential reaction of 3,6-diacetylpyridazine (**7**) with sodium hydride, carbon disulfide, and *n*-propyl iodide. Compound **9** was allowed to react with the ketone enolate generated from 2-acetylpyridine and sodium hydride to yield 24% of the mono-coupled product **10** and 7% of the bis-coupled product **11** following ring closure with ammonium acetate. The reaction of the Michael acceptor **10** with the sodium hydride generated ketone enolate of the unsymmetrically substituted pyridazine **8** gave **12** in 33% yield following ring closure with ammonium acetate. Subsequent hydrolysis of **12** in aqueous acid gave **13** in 97% yield. Reaction of 2.4 equivalents of **13** with the bis-Michael acceptor **9** led to the desired final product **3** in 19% yield.

The general concept of helicity codons: The sequence of primary, secondary, tertiary, and quaternary structure in proteins is an excellent example of hierarchical self-organization in nature. Proteins rely on various combinations of amide bonds, disulfide bridges, hydrogen bonds, ionic and dipole–dipole interactions, as well as hydrophobic effects to control their final three-dimensional structure. In essence, biological polypeptides are linear polymers whose conformation and properties are encoded within a given sequence of the twenty constituent amino acid monomers. This same premise holds true for suitably designed oligoheterocyclic strands where specific subunits (such as the α,α' -pyridine–pyrimidine group^[6–11]) act as *helicity codons* that enforce helical winding due to the highly preferred *transoid* conformation around the α,α' -interheterocyclic bonds.^[6, 8–13] In the particular case of compound **3**, molecular modeling starting from an extended non-helical form yields as optimal conformation a helical structure having approximately ten heterocycles per turn with the two terminal pyridine rings overlapping at about 3.4 Å (Figure 1) and an internal void of about 8 Å diameter.

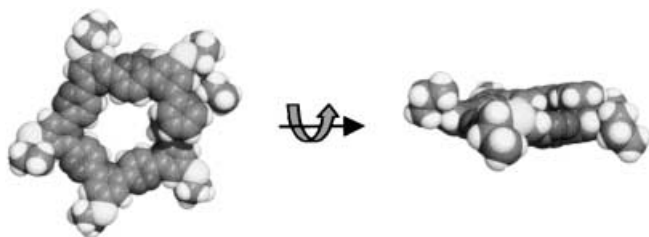


Figure 1. Minimized conformation of compound **3** viewed face-on and from the side, calculated by using the CVFF95 force field with the Cerius2 package.

The importance of intramolecular aromatic stacking in chloroform is clearly indicated since there are almost three rings overlapping in the computationally optimized helical structure as opposed to one ring overlap in the geometrically optimized structure without the solvent.

The intramolecular features responsible for folding include: 1) weak favorable hydrogen bond interactions between the lone pair of electrons on the nitrogen and the opposite hydrogen atom on the neighboring heterocycle in the *transoid*

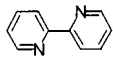
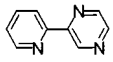
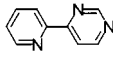
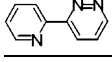
conformer, 2) favorable antiparallel orientation of the nitrogen dipoles in the *transoid* conformer, 3) unfavorable steric *ortho*-H/*ortho*-H' interactions in the *cisoid* conformer, and 4) favorable π – π stacking and van der Waals interactions between heterocyclic rings once a turn of the helix is complete.

The simultaneous action of these different interactions results in the requisite coplanarity and *transoid* conformation between neighbouring heterocycles and provides the driving force for the stabilization of helical structures. The α,α' -interheterocyclic bond is thus remarkably similar to the dipeptide bond in proteins, whose partial double-bond character imposes a coplanar, and normally *transoid*, CO–NH bond conformation.^[31] As a further indication of the generality of intramolecular conformational control based on heterocyclic connectivity, the rings of the central tetraazaterphenyl moiety in 4-phenylenebis(5-phenyl-2-pyrimidine) have been shown to be almost coplanar with an interheterocyclic twist angle of about 8°.^[32] In all these cases, the structural and conformational information encoded in the molecular strands allows a programmed molecular self-organization process directed by intramolecular noncovalent interactions.^[6–11]

To evaluate the driving force for helix formation, we calculated, using density functional theoretical models, the energy difference between the *cisoid* (planar), *cisoid* (nonplanar), and *transoid* conformers of 2,2'-bipyridine, 2-pyridin-2-yl-pyrazine, 4-pyridin-2-yl-pyrimidine, and 3-pyridin-2-yl-pyridazine (Table 1). The corresponding barriers for *cis/trans* interconversion were also obtained. In all cases the *transoid* conformer is 6–7 kcal mol^{−1} lower in energy than the lowest energy *cisoid* conformer. The contribution of interheterocyclic dipole–dipole interactions to the *cisoid*–*transoid* energy differences can be appreciated from the comparison of the dipole moments of the individual heterocyclic units in 2-pyridin-2-yl-pyrazine with those in 2,2'-bipyridine, 4-pyridin-2-yl-pyrimidine, and 3-pyridin-2-yl-pyridazine: $\mu_{\text{pyridine}} = 2.22$ D; $\mu_{\text{pyridazine}} = 4.22$ D; $\mu_{\text{pyrimidine}} = 2.33$ D; $\mu_{\text{pyrazine}} = 0$ D.

Thus, the 2-pyridin-2-yl-pyrazine shows the lowest energy barrier and the smallest *cisoid*–*transoid* energy difference due to the small dipole moment of the pyrazine fragment. The larger energy differences are obtained when a pyridazine

Table 1. The relative energy difference (in kcal mol^{−1}) between the planar *cisoid*, the nonplanar *cisoid* and *transoid* conformers of 2,2'-bipyridine, 2-pyridin-2-ylpyrazine, 4-pyridin-2-ylpyrimidine, and 3-pyridin-2-ylpyridazine calculated by using the B3LYP density functional theory with a triple zeta basis set including polarization functions for all atoms and diffuse functions just for carbon and nitrogen atoms (B3LYP/6–311 + G** level of theory).

Compound	<i>cisoid</i> (planar)	<i>cisoid</i> (nonplanar)	Barrier	<i>transoid</i>
	+ 8.3	+ 6.5	+ 7.6	0.0
	+ 7.5	+ 5.7	+ 7.0	0.0
	+ 8.0	+ 6.6	+ 7.8	0.0
	+ 9.4	+ 7.3	+ 8.0	0.0

group is involved, that is with the individual heterocyclic unit presenting the strongest dipole moment. These calculations further confirm the marked preference for a planar arrangement of the α,α' connected bis-heterocyclic unit with a *transoid* conformation.

Intra- and intermolecular interactions of compound 3: Compound **11**, a side product in our synthetic sequence, forms less than one half turn of a helix and was used as a control to monitor helix formation in compound **3**. A significant upfield shift of the proton resonance signals at positions C4 and C5 of the terminal pyridine rings is observed when comparing the NMR spectra of **11** and **3** (Figure 2).

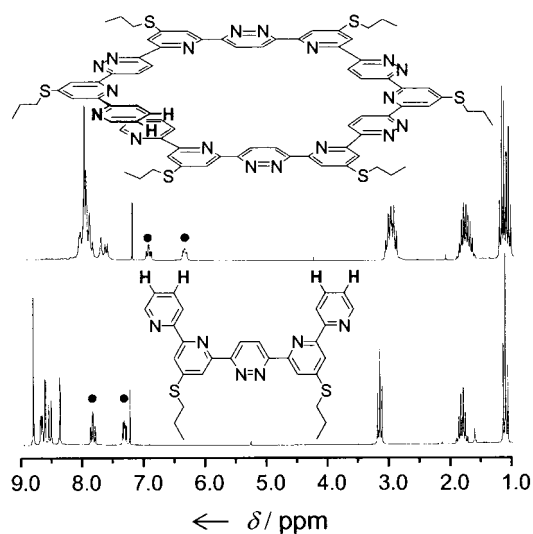


Figure 2. ^1H NMR spectra (200 MHz) of compound **11** (bottom) at 25°C and compound **3** (top) in CDCl_3 at 55°C . The proton resonances at positions C4 and C5 of the terminal pyridyl rings are highlighted.

This marked shielding, due to the overlap of the heteroaromatic groups, confirms the helical conformation of compound **3** in solution and is also diagnostic of helix formation in strands of repeating pyridine–pyrimidine units,^[6–11] helicenes,^[33] and heterohelicenes.^[34]

Furthermore, it was found that all aromatic proton resonances of compound **3** in chloroform are shifted to higher fields as the concentration is increased. At 55°C the chemical shifts of the aromatic signals vary dramatically as the concentration is changed from 0.4 mM to 31.2 mM, while those of the aliphatic protons remain relatively unchanged over the same concentration range (Figure 3). This observation is indicative of the formation of molecular assemblies resulting in diamagnetic anisotropy effects between neighboring molecules. Assuming a monomer–dimer equilibrium, it was possible to determine a dimerization constant, K_{assoc} , by monitoring the shift of the terminal pyridine C4 and C5 proton signals over a concentration range of 0.1 to 100 mM at 35°C using curve fitting methods described for analyzing the aggregation of phenylacetylene macrocycles^[35] (Figure 4). Values of 5200 M^{-1} and 6700 M^{-1} were obtained by using the C3 and C4 protons on the terminal pyridine ring. These high

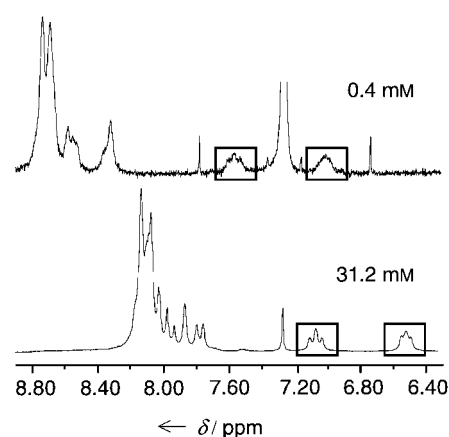


Figure 3. Concentration dependence of ^1H NMR spectra (200 MHz) of compound **3** in CDCl_3 at 55°C . The proton resonances at positions C4 and C5 of the terminal pyridyl rings are highlighted.

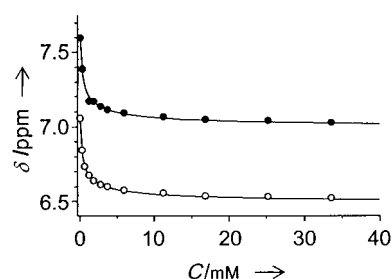


Figure 4. Concentration C dependence of ^1H NMR (200 MHz) chemical shifts for the terminal pyridine C4 and C5 proton signals of compound **3** in CDCl_3 over a concentration range of 0.1 to 100 mM at 35°C (data points at 50.3 mM and 100.7 mM are not shown).

association constants suggest the formation of self-assembled dimers through face-to-face π – π interactions between the aromatic heterocycles of neighboring molecules in either a head-to-head double helix or a head-to-tail single helix. As a consequence, the observed shifts of the proton resonances at positions C4 and C5 of the terminal pyridine rings incorporate contributions from both intra- and intermolecular π – π stacking components.

Self-aggregation was further confirmed by vapor pressure osmometry which yielded an apparent molecular weight for compound **3** of about 3600 g mol^{-1} (at 36°C in chloroform over a concentration range of 2–18 mM; Figure 5). This value is about 2.5 times the actual molecular weight of $1453.92\text{ g mol}^{-1}$ of the monomer and suggests that higher order aggregates beyond dimerization are not prevalent in these conditions.

Force field calculations, obtained using CVFF95 with the Cerius2 package, gave the relative stabilities of both the head-to-tail stacked helical dimer and the head-to-head interlocked helical dimer (Figure 6). Intermolecular electrostatic interactions slightly favor the head-to-tail dimer by 4 kcal mol^{-1} in vacuum and by 1.5 kcal mol^{-1} in CHCl_3 . These differences in relative stability are too small to draw any conclusions based on such type of calculations. One may however note that,

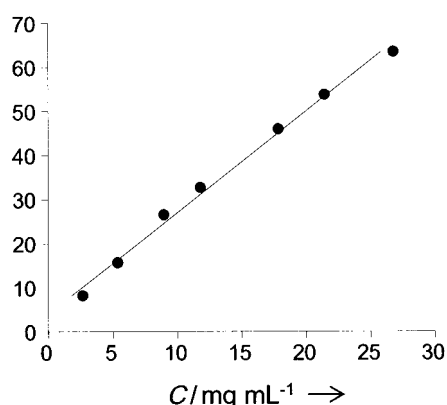


Figure 5. Vapor pressure osmometry of compound **3** at 36 °C in CHCl_3 over a concentration (C) range of 2–18 mM. Change in voltage (ΔV) plotted versus the osmotic concentration of compound **3** in mg mL^{-1} . An instrument calibration constant of 11 262 was obtained from a calibration curve obtained with a polystyrene molecular weight standard ($\text{MW} = 2430$, $\text{MN}_{\text{VPO}} = 2330$).

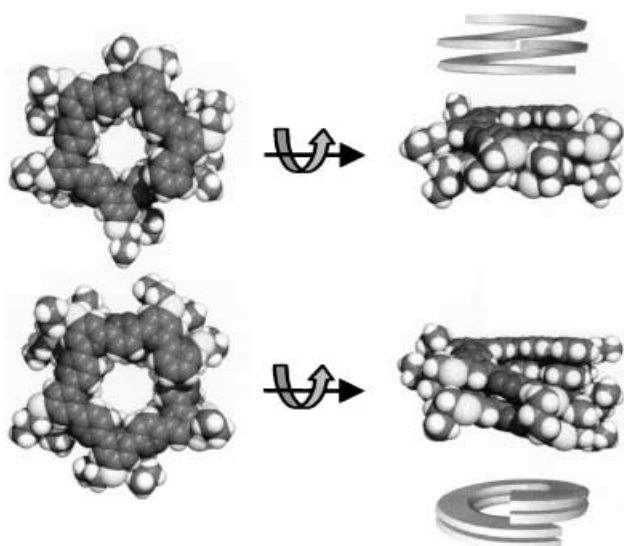


Figure 6. Minimized conformation of head-to-tail stacked helical dimer (above) and the head-to-head double helical dimer (below) of compound **3** viewed face-on and from the side, calculated using the CVFF95 force field with the Cerius2 package. Schematic representations of the types of dimers are shown.

whatever the details of their structure, such dimeric species represent the first step in the formation of multi-unit stacks that possess an interval void conferring upon them features of a molecular channel (see below).

Hierarchical and cooperative self-assembly of compound **3** into supramolecular protofibrils, fibrils, and macrofibers:

Low molecular weight gelators for organic solvents generate elongated aggregates which subsequently assemble into fibrous structures that form an extended entangled network. Currently there is significant interest in the syntheses of functionalized and aggregating helical conjugated molecules.^[36] Compound **3** was found to produce a gel at a concentration of 1 mg mL^{-1} in dichloromethane. This observation prompted an electron microscopic investigation which revealed extensive fiber network formation with helical

substructures. The freeze fracture electron micrographs of **3** in dichloromethane and pyridine (Figure 7) reveal uniform helical fibrils with an approximate diameter of 55–70 Å. Networks of fibrils of micrometer length subsequently form linear and intertwined fibers and macrofibers.

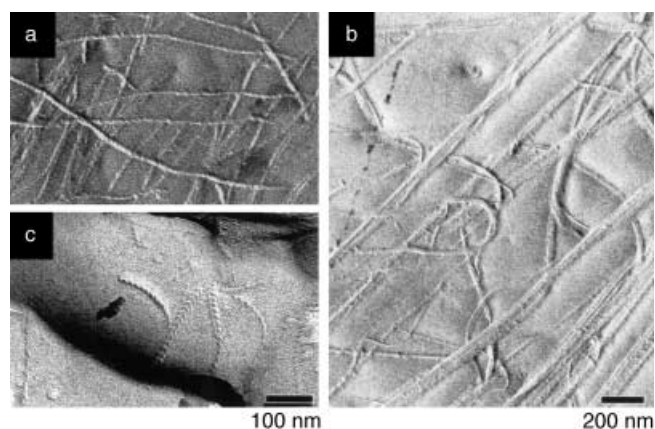


Figure 7. Freeze-fracture electron micrographs of compound **3** in a, b) dichloromethane (0.5 mg mL^{-1}) and c) pyridine (2 mg mL^{-1}) showing fibril network formation with helical textures (a, c) and molecular aggregation into linear and helical fibers and macrofiber bundles (c).

A possible model would imply that the self-organized lock-washer structures of compound **3** first stack to form cablelike protofibrils or filaments (not observed in our micrographs). These filaments further aggregate into fibrils (likely composed of coiled-coil bundles of two or three single molecular stacks) that subsequently aggregate into larger bundles and align and twist to form mature fibers (Figure 8). Such a

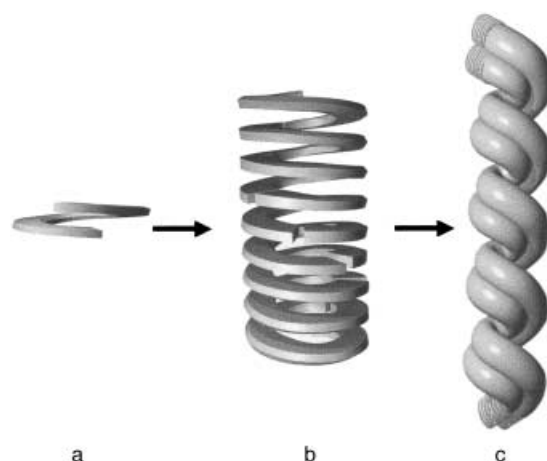


Figure 8. Schematic representation of the hierarchical self-assembly of compound **3**. The self-organized lock-washer structure (a) of **3** is proposed to self-assemble to form protofibrils or filaments (b), and fibrils (c).

behavior is reminiscent of the self-aggregation of collagen (where three polypeptide chains fold into a triple-helical conformation to form collagen monomers which subsequently self-assemble into cablelike collagen fibers)^[37, 38] and of the evolution of oligomeric intermediates in amyloid fibrillogenesis thought to occur through specific intermolecular

interactions between partially ordered protein conformations.^[39, 40]

The chirality observed in the fibrils, manifested as helical twisting, could result from favorable intermolecular π – π stacking interactions from helices of compound **3** of the same helical sense. The molecular helical chirality is subsequently translated into supramolecular helicity that is expressed on a nanoscale. In dichloromethane, a dominance of fibers of the same chirality is apparently observed; it may be due to the induction of fiber formation by chiral seeds originating from the sonication-induced breakdown of an initial helical entity. This observation is reminiscent of the results of a recent report of amplification of prion protein aggregates, where sonication is used to generate smaller free units of misfolded protein to serve as templates for further growth.^[41] Very well-defined helical structures displaying left- and right-handed helical twists were observed from the birefringent solution of compound **3** in pyridine (2 mg mL^{-1}). The interlocked stacking of the helically wound strands of compound **3** bears also relation to the in vitro self-association of the tobacco mosaic virus lock-washer assemblies into an extended helical rod.^[42] This molecular aggregation into protofibrils, fibrils, and macrofiber bundles is not dissimilar to gels obtained from crown-ether-substituted phthalocyanines.^[43]

Langmuir–Blodgett and cast thin films of compound **3**:

Recent interest in Langmuir films composed of nontraditional amphiphiles, in particular disc-shaped molecules,^[36, 44] prompted us to study Langmuir–Blodgett films of compound **3**. A typical pressure–area isotherm for **3** at the air–water interface is shown in Figure 9. The isotherm yields a limiting

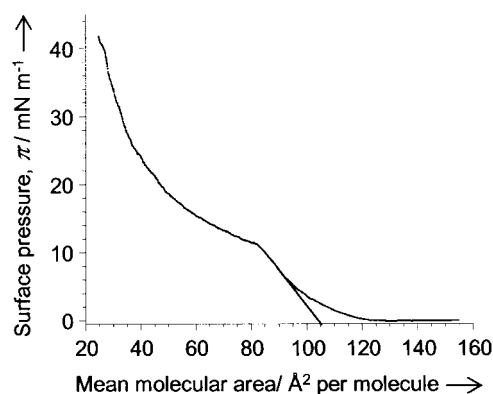


Figure 9. Pressure–area isotherm for compound **3** at the air–water interface (22°C ; barrier speed: 2 mm min^{-1}) showing a limiting area of about $105 \text{ \AA}^2 \text{ molecule}^{-1}$.

area of about $105 \text{ \AA}^2 \text{ molecule}^{-1}$. Depending on the conformation of the alkyl chains, compound **3** in a helical self-organized state has an outside diameter of about 25 \AA and a thickness of about 5 \AA . In an 'edge-on' arrangement (perpendicular to the water surface) a molecular area of about $125 \text{ \AA}^2 \text{ molecule}^{-1}$ results, in rather good agreement with the measured limiting area of about $105 \text{ \AA}^2 \text{ molecule}^{-1}$. This is in accord with a general rule for disc-shaped molecules where molecules with strong core–core attractions favor the 'edge-on' arrangement.^[45] As shown above, compound **3** does

indeed show strong intermolecular interactions. A face-on arrangement with the helix parallel to the water surface would result in a significantly larger cross-sectional area.

Tapping-mode atomic force microscopy images of Langmuir–Blodgett films of compound **3** deposited on mica at various points along the isotherm are shown in Figure 10. The monolayers are featureless and have a constant thickness of

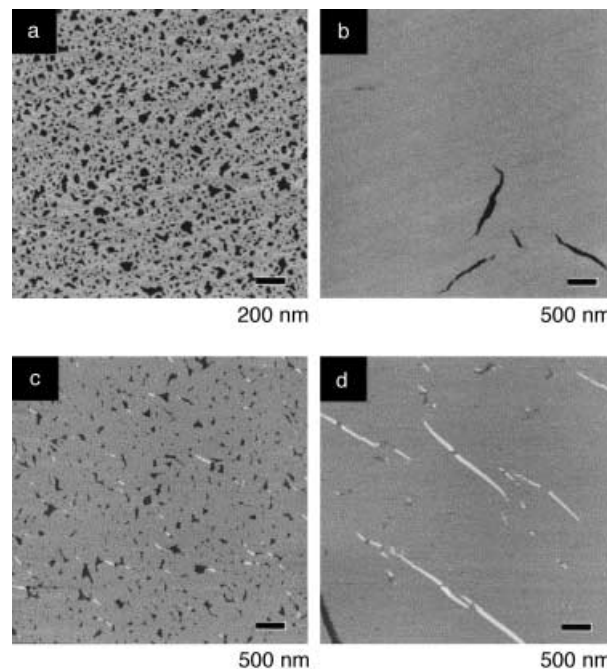


Figure 10. Tapping-mode AFM images of Langmuir–Blodgett films of compound **3** deposited on mica at a) 5 mN m^{-1} , b) 10 mN m^{-1} , c) 15 mN m^{-1} , and d) 30 mN m^{-1} . The total height range is 10 nm for a & b and 20 nm for c & d.

about 22 \AA . This is also consistent with compound **3** oriented perpendicularly (i.e. edge-on) or slightly tilted with respect to the water surface. The surface coverage increases as the surface pressure increases, and as the pressure increases beyond 10 mN m^{-1} , multilayer formation becomes increasingly evident. The multilayer thickness is also constant and has a value of about 50 \AA above the monolayer. This thickness can perhaps be attributed to a buckling of the monolayer to form bilayer structures on top of the pre-existing monolayer. We attribute the shoulder in the Langmuir isotherm at about 12 mN m^{-1} to multilayer formation. This shoulder was variable from isotherm to isotherm and was found to be dependent on such factors as the age and concentration of the spreading solution, the amount of material spread on the trough, and the time allowed for solvent evaporation. These factors can be related to the propensity of compound **3** to self-aggregate to varying extents. Similar variability has been reported in the Langmuir isotherms of octasubstituted phthalocyanines.^[46]

The Langmuir isotherms were irreversible (i.e. the film does not relax to its precompressed state) and the transfer ratios were extremely variable (0% to 80%). However, AFM imaging of different samples prepared at the same pressure were reproducible. It has previously been reported that accurate determination of transfer ratios for octasubstituted

phthalocyanin Langmuir–Blodgett films is difficult due to their rigidity in the fully compressed state.^[47, 48] The following observations give evidence that the Langmuir films formed from compound **3** are very rigid: 1) during film compression above about 20 mNm⁻¹, wrinkles on the water surface were observed near the edge of the moving barrier, 2) if the Whilhemy plate was oriented parallel to the barrier, the Langmuir film at higher pressures was able to cause the filter plate to tilt, 3) one can often observe fragments of complementary shapes in the AFM images (not shown).

Compound **3** was also found to form ordered thin films on mica from organic solution. Tapping-mode AFM images of cast films of **3** on freshly cleaved mica are represented in Figure 11. The micrograph in Figure 11a shows surface

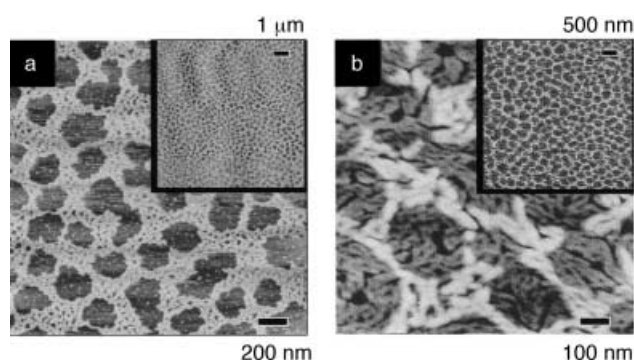


Figure 11. Tapping-mode AFM images of cast films of compound **3** on freshly cleaved mica (a 5 μ L drop of a 0.274 mgmL⁻¹ CHCl₃ solution). Micrograph a) shows surface patterns at submonolayer coverage and micrograph b) shows surface patterns at multilayer coverage with wormlike substructures. The insets show large scale images of the same areas. The total height range for all images is 10 nm.

patterns with submonolayer coverage. The height of the monolayer is about 20 Å which is consistent with the thickness of the monolayers formed by using the Langmuir–Blodgett technique. Although the sample preparation for the micrograph in Figure 11b was identical to those of Figure 11a, in this case multilayer coverage was observed. The height of the first layer is about 20 Å, while the second layer is about 30 Å higher than the first layer. The interesting feature in this case is the wormlike substructure observed in both layers. The horizontal dimension of these elements is about 20 nm. Although the relationship between these wormlike substructures and the fibers observed in the electron micrographs is uncertain, it is clear that compound **3** has a diverse ability to self-assemble and form both two- and three-dimensional supramolecular structures.

Conclusion

The synthesis and characterization of an alternating pyridine–pyridazine molecular strand **3** comprising thirteen heterocycles was described. Compound **3** was designed to wind into a helical structure enforced by the conformational features of the subunits and possessing a rather large internal void of about 8 Å diameter. It undergoes hierarchical self-

assembly successively into supramolecular protofibrils, fibrils, and fibers. Particularly attractive in this *self-organizing/self-assembling* system is the formation of bundles of extended molecular channels constituted by tubular (helical) stacks with hollow cores of finite size, thus opening ways for the design of functional polymolecular materials for *multi-channel* ion-active devices. Further developments towards this end involve internal functionalization with ion binding sites.^[13] Analogous to the primary amino acid sequence encoding the required information for protein folding and assembly, the primary heterocyclic sequence and connectivity encodes for helical molecular self-organization and subsequent supramolecular self-assembly in both two and three dimensions. Such systems represent an implementation of basic structural design principles for enforcing controlled, sequential and hierarchical self-organization processes generating well-defined polymolecular functional devices at the supramolecular level.

Experimental Section

General procedures: Dimethylformamide (DMF) was purchased anhydrous and used without further purification. Tetrahydrofuran (THF) was distilled under argon from sodium benzophenone immediately prior to use. Dimethyl sulfoxide (DMSO) was distilled over CaH₂ in vacuo and stored over activated 4 Å molecular sieves. 2-Acetylpyridine was purchased from Aldrich and used without further purification. Tributyl-(1-ethoxyvinyl)tin was prepared according to a published procedure.^[49] *trans*-Bis(triphenylphosphine)palladium(II) chloride (19.83 g, 28.0 mmol) was prepared in 93 % yield from palladium(II) chloride (5.32 g, 30.0 mmol) and triphenylphosphine (15.75 g, 59.4 mmol) by stirring in DMSO at room temperature overnight, filtering on a glass frit, and washing successively with THF and hexane. Chromatography was carried out on Merck 60 silica gel (0.040–0.063 mm), Merck activity II–III aluminum (0.063–0.200 mm), and aluminium oxide 60 PF254 (type E) for preparative layer chromatography. Melting points were recorded on an electrothermal digital melting point apparatus and are uncorrected. Infrared absorption spectra were measured on a Perkin–Elmer 1600 series FTIR spectrometer as KBr disks or as a neat film on a NaCl disk. ¹H and ¹³C NMR were recorded on a Bruker AC200 or a Bruker ARX 500 spectrometer in CDCl₃. The chemical shifts were calibrated to the residual solvent peak. FAB-mass spectrometric measurements were performed by the Service de Spectrométrie de Masse (Institut de Chimie, Université Louis Pasteur), and elemental analyses were carried out by the Service de Microanalyse (Institut de Chimie, Université Louis Pasteur).

Energy calculations and molecular modelling: The energy difference between the *cisoid* and *transoid* conformers of 2,2'-bipyridine, 2-pyridin-2-yl-pyrazine, 4-pyridin-2-yl-pyrimidine, and 3-pyridin-2-yl-pyridazine was calculated by using the B3LYP density functional theory with a triple zeta basis set including polarization functions for all atoms and diffuse functions just for carbon and nitrogen atoms (B3LYP/6–311 + G** level of theory). Force field calculations using CVFF95 with the Cerius2 package were used to determine the optimal conformation of compound **3** and to obtain the relative stabilities of both the head-to-tail stacked helical dimer and the head-to-head interlocked helical dimer in CDCl₃.

Vapor pressure osmometry: Molecular weight determinations were performed with a Knauer (Berlin, Germany) twin thermister hanging drop vapor pressure osmometer operated at 36 °C. The molecular weight of compound **3** was measured in HPLC grade chloroform in a concentration range of 2–18 mM. A calibration curve was generated by using a polystyrene molecular weight standard (MW = 2430, M_N_{VPO} = 2330, polydispersity = 1.06).

Electron microscopy: Organogels for freeze fracture transmission electron microscopy were prepared by dissolving compound **3** (0.5–2.0 mg) in dichloromethane or pyridine with heating and bath sonication. The

solutions were aged at room temperature for at least 12 h prior to use. Freeze fracture experiments were performed in an apparatus developed at IGBMC by J.-C. Homo. Gel solutions were sandwiched between two copper specimen holders and frozen in liquid nitrogen. The frozen samples were transferred to the fracture replication stage which was kept at a vacuum of 10^{-8} mbar at -178°C . Replication was performed immediately after fracturing with about 20 Å platinum/carbon at 45° followed by about 200 Å carbon at 90° . The replicas were retrieved and cleaned in chloroform, mounted on carbon-coated grids, and observed with a Philips CM12 electron microscope operating at 100 keV.

Langmuir and Langmuir–Blodgett films: Langmuir and Langmuir–Blodgett films were prepared at 23°C on a Nima Technology (Coventry, UK) type 611 Langmuir–Blodgett trough (length = 27 cm, width = 10 cm; open area = 270 cm^2 , closed area = 40 cm^2) with a barrier speed of 2 mm min^{-1} , equipped with a Whilhem balance (10 mm width filter paper). All films were prepared on a water subphase purified by using a MilliPore Milli-Q system by spreading $150\text{ }\mu\text{L}$ of a dilute solution of **3** (0.274 mg mL^{-1}) on the water surface and allowing one hour for solvent evaporation. Langmuir–Blodgett films were prepared on freshly cleaved HI-GRADE mica sheets (Ted Pella, Inc., Redding, CA) with a dipping rate of 1 mm min^{-1} in the upward direction through the monolayer, beginning in the subphase.

Atomic force microscopy (AFM): A Nanoscope IIIa Multimode scanning probe microscope, from Digital Instruments (Santa Barbara, CA) was used for Langmuir–Blodgett and thin film microscopic characterization. The atomic force microscope was operated in the tapping mode using $125\text{ }\mu\text{m}$ etched silicon probes (Digital Instruments Nanoprobe TESP) used as received with a drive frequency between 320 and 340 KHz. The scan rate was either 0.5 or 1.0 Hz. Solvent cast films were prepared from a $5\text{ }\mu\text{L}$ drop of a 0.274 mg mL^{-1} solution of **3** in CHCl_3 ; the solvent was allowed to evaporate slowly under a beaker. Freshly cleaved HI-GRADE mica (Ted Pella, Inc., Redding, CA) was used as the substrate. The images shown are flattened but otherwise unmodified.

3-Chloro-6-(1-ethoxyvinyl)pyridazine (4): Tributyl-(1-ethoxyvinyl)tin (80.0 g, 0.22 mol), 3,6-dichloropyridazine (34.8 g, 0.23 mol), *trans*-bis(triphenylphosphine)palladium(II) chloride (7.5 g, 10.7 mmol), and DMF (150 mL) were combined in a 250 mL round-bottom flask. The flask was purged with argon and stirred at 80°C for 18 h. The resulting dark solution was allowed to cool to room temperature and poured into a flask containing KF (35 g) in water (300 mL). Diethyl ether (200 mL) was then added and the mixture was stirred vigorously for 30 min, filtered, and the solid washed well with diethyl ether. The organic phase was collected, washed with water ($2 \times 300\text{ mL}$), dried over sodium sulfate, and evaporated on a rotary evaporator to yield a dark oil which was purified by column chromatography (silica, hexane/diethyl ether (95% v/v) followed by hexane/acetone (90% v/v) eluent). The fractions containing the product were combined, and the solvent removed to yield 28.2 g of the crude product which was recrystallized from hexane to give **4** (22.0 g; 54% yield) as colorless plates. M.p. $72.9\text{--}73.9^{\circ}\text{C}$; R_f (silica, CH_2Cl_2): 0.28; $^1\text{H NMR}$ (200 MHz, CDCl_3 , 25°C): $\delta = 7.75$ (d, $J = 8.9\text{ Hz}$, 1H), 7.46 (d, $J = 8.9\text{ Hz}$, 1H), 5.66 (d, $J = 2.4\text{ Hz}$, 1H), 4.47 (d, $J = 2.4\text{ Hz}$, 1H), 3.95 (q, $J = 7.0\text{ Hz}$, 2H), 1.39 ppm (t, $J = 7.0\text{ Hz}$, 3H); $^{13}\text{C NMR}$ (50 MHz, CDCl_3 , 25°C): $\delta = 155.97$, 155.75, 154.90, 128.15, 125.09, 87.24, 63.90, 14.47 ppm; IR (KBr): $\tilde{\nu} = 3083$, 2989, 2926, 2880, 1621, 1565, 1528, 1480, 1461, 1412, 1395, 1305, 1159, 1137, 1077, 1050, 974, 877, 854, 816 cm^{-1} ; MS (FAB+): m/z : 185.0 (100%, MH^+); elemental analysis calcd (%) for $\text{C}_8\text{H}_9\text{N}_2\text{OCl}$ (184.63): C 52.05, H 4.91, N 15.17; found: C 52.17, H 4.97, N 15.36.

3,6-Bis-(1-ethoxyvinyl)pyridazine (5): Tributyl-(1-ethoxyvinyl)tin (90.0 g, 0.25 mol), 3,6-dichloropyridazine (17.2 g, 0.12 mol), *trans*-bis(triphenylphosphine)palladium(II) chloride (7.5 g, 10.7 mmol), and DMF (150 mL) were combined in a 250 mL round-bottom flask and allowed to react as described for the preparation of **4** to give an orange oil (15.4 g; 58% yield) after chromatography. This product was used in the subsequent reaction as such. An analytically pure sample of **5** was obtained after a second silica column (dichloromethane/ethyl acetate (95% v/v) eluent). R_f (silica, CH_2Cl_2): 0.15; $^1\text{H NMR}$ (200 MHz, CDCl_3 , 25°C): $\delta = 7.76$ (s, 2H), 5.77 (d, $J = 2.2\text{ Hz}$, 2H), 4.47 (d, $J = 2.2\text{ Hz}$, 2H), 3.98 (q, $J = 7.0\text{ Hz}$, 4H), 1.42 ppm (t, $J = 7.0\text{ Hz}$, 6H); $^{13}\text{C NMR}$ (50 MHz, CDCl_3 , 25°C): $\delta = 155.94$, 155.34, 122.52, 86.42, 63.65, 14.54 ppm; IR (neat film): $\nu = 2980$, 2931, 1621, 1574, 1531, 1479, 1443, 1401, 1368, 1302, 1160, 1089, 1060, 974, 863, 824 cm^{-1} ; MS (FAB+): m/z : 221.0 (100%, MH^+); elemental analysis calcd (%) for

$\text{C}_{12}\text{H}_{16}\text{N}_2\text{O}_2$ (220.27): C 65.43, H 7.32, N 12.72; found: C 65.66, H 7.48, N 12.80.

3-Chloro-6-acetylpyridazine (6): Compound **4** (21.0 g, 0.114 mol) was dissolved in acetone (50 mL) and 2N HCl (25 mL) and the solution stirred overnight at room temperature. The precipitate was filtered from the solution and washed with aqueous sodium hydrogen carbonate and water to give an off-white product (14.1 g; 79% yield). This product was used in the subsequent reaction as such. An analytically pure sample of **6** was obtained after recrystallization from hexane. M.p. $123.2\text{--}124.3^{\circ}\text{C}$; R_f (silica, CH_2Cl_2): 0.32; $^1\text{H NMR}$ (200 MHz, CDCl_3 , 25°C): $\delta = 8.06$ (d, $J = 8.8\text{ Hz}$, 1H), 7.66 (d, $J = 8.8\text{ Hz}$, 1H), 2.81 ppm (s, 3H); $^{13}\text{C NMR}$ (50 MHz, CDCl_3 , 25°C): $\delta = 197.36$, 159.53, 154.98, 129.14, 127.04, 26.03 ppm; IR (KBr): $\tilde{\nu} = 3380$, 3078, 3056, 2926, 1697, 1561, 1401, 1362, 1332, 1259, 1152, 1108, 1046, 962, 858 cm^{-1} ; MS (FAB+): m/z : 157.0 (100%, MH^+); elemental analysis calcd (%) for $\text{C}_8\text{H}_8\text{N}_2\text{OCl}$ (156.57): C 46.03, H 3.22, N 17.89; found: C 46.23, H 3.35, N 18.00.

3,6-Diacetyl-pyridazine (7): Compound **5** (13.7 g, 62 mmol) was dissolved in acetone (50 mL) and 2N HCl (25 mL) and allowed to react as described for the preparation of **6** to give **7** as a yellow product (7.9 g; 77% yield). This product was used in the subsequent reaction as such. An analytically pure sample of **7** was obtained after recrystallization from hexane and sublimation (70°C , 0.03 mm Hg). M.p. $150.4\text{--}150.8^{\circ}\text{C}$; R_f (silica, CH_2Cl_2): 0.22; $^1\text{H NMR}$ (200 MHz, CDCl_3 , 25°C): $\delta = 8.21$ (s, 2H), 2.88 ppm (s, 6H); $^{13}\text{C NMR}$ (50 MHz, CDCl_3 , 25°C): $\delta = 197.56$, 156.59, 125.66, 26.33 ppm; IR (KBr): $\tilde{\nu} = 3384$, 3062, 2931, 1703, 1570, 1416, 1377, 1358, 1342, 1278, 1248, 1128, 1097, 1041, 1017, 963, 870 cm^{-1} ; MS (FAB+): m/z : 165.1 (100%, MH^+); elemental analysis calcd (%) for $\text{C}_8\text{H}_8\text{N}_2\text{O}_2$ (164.16): C 58.53, H 4.91, N 17.06; found: C 58.71, H 4.95, N 17.15.

3-Acetyl-6-(1-ethoxyvinyl)pyridazine (8): Tributyl-(1-ethoxyvinyl)tin (36 g, 100 mmol), **6** (12 g, 77 mmol), *trans*-bis(triphenylphosphine)palladium(II) chloride (2.4 g, 3.9 mmol), and DMF (50 mL) were combined in a 250 mL round-bottom flask. The flask was purged with argon and stirred at 80°C for 18 h. The resulting dark solution was allowed to cool to room temperature and poured into a flask containing KF (10 g) in water (100 mL). Diethyl ether (100 mL) was then added and the mixture was stirred vigorously for 30 min, filtered, and the solid washed well with diethyl ether. The organic phase was collected, washed with water ($2 \times 100\text{ mL}$), dried over sodium sulfate, and evaporated on a rotary evaporator to yield a dark oil which was purified by column chromatography (silica, hexane/diethyl ether (95% v/v) eluent). The fractions containing the product were combined, and the solvent removed and the yellow solid thus obtained was further purified by vacuum sublimation at 75°C to give **8** (12.3 g; 83% yield). This product was used in the subsequent reaction as such. An analytically pure sample of **8** was obtained after recrystallization from hexane. M.p. $78.6\text{--}79.4^{\circ}\text{C}$; R_f (silica, CH_2Cl_2): 0.20; $^1\text{H NMR}$ (200 MHz, CDCl_3 , 25°C): $\delta = 8.10$ (d, $J = 8.8\text{ Hz}$, 1H), 7.93 (d, $J = 8.8\text{ Hz}$, 1H), 5.90 (d, $J = 2.4\text{ Hz}$, 1H), 4.62 (d, $J = 2.4\text{ Hz}$, 1H), 4.01 (q, $J = 7.0\text{ Hz}$, 2H), 1.44 ppm (t, $J = 7.0\text{ Hz}$, 3H); $^{13}\text{C NMR}$ (50 MHz, CDCl_3 , 25°C): $\delta = 198.38$, 157.92, 155.31, 154.94, 125.02, 123.11, 88.93, 63.94, 26.16, 14.47 ppm; IR (KBr): $\tilde{\nu} = 3056$, 2986, 1698, 1624, 1568, 1540, 1421, 1384, 1360, 1332, 1306, 1270, 1153, 1116, 1066, 958, 875, 842 cm^{-1} ; MS (FAB+): m/z : 193.0 (100%, MH^+); elemental analysis calcd (%) for $\text{C}_{10}\text{H}_{12}\text{N}_2\text{O}_2$ (192.22): C 62.49, H 6.29, N 14.57; found: C 62.44, H 6.29, N 14.40.

3,6-Bis-[1-(3,3-bis-propylsulfanyl)acryloyl]pyridazine (9): Compound **7** (6.12 g, 37.3 mmol) was dissolved in dry DMSO (200 mL) in a 500 mL flask under nitrogen and cooled with a water bath. NaH (6.5 g 60% w/w in mineral oil, 162.5 mmol) was added to the solution over a 10 min period followed by the dropwise addition of CS_2 (5.7 g, 75.0 mmol) by a syringe over a 20 min period. *n*PrI (25.5 g, 150.0 mmol) was subsequently added dropwise by a syringe over a period of 30 min. The dark brown mixture was stirred at room temperature for 19 h and poured into water (1 L). The mixture was extracted with CHCl_3 ($3 \times 500\text{ mL}$). The combined organic phases were reduced in volume with a rotary evaporator and washed with water ($2 \times 200\text{ mL}$). The organic phase was collected, dried over sodium sulfate, and evaporated on a rotary evaporator and was purified by column chromatography (alumina, dichloromethane eluent). The fractions containing the product were combined and the solvent removed to yield the crude product (14 g) which was washed with hexanes and recrystallized from ethanol to give **9** (11.9 g; 66% yield) as golden needles. M.p. $157.5\text{--}158.6^{\circ}\text{C}$; R_f (silica, CH_2Cl_2): 0.18; R_f (alumina, CH_2Cl_2): 0.63; $^1\text{H NMR}$ (200 MHz, CDCl_3 , 25°C): $\delta = 8.37$ (s, 2H), 7.80 (s, 2H), 3.12 (m, 8H), 1.80

(m, 8H), 1.09 ppm (m, 12H); ^{13}C NMR (50 MHz, CDCl_3 , 25 °C): δ = 181.07, 170.48, 157.80, 126.82, 108.93, 36.48, 33.76, 22.33, 20.90, 13.70 ppm; IR (KBr): $\tilde{\nu}$ = 2964, 2929, 2872, 1622, 1545, 1472, 1404, 1239, 1223, 1100, 1080, 981, 804 cm^{-1} ; MS (FAB +): m/z : 485.1 (100%, MH^+); elemental analysis calcd (%) for $\text{C}_{22}\text{H}_{32}\text{N}_2\text{O}_2\text{S}_4$ (484.75): C 54.51, H 6.65, N 5.78; found: C 54.53, H 6.46, N 5.72.

3,3-Bis-propylsulfanyl-1-[6-(4-propylsulfanyl-[2,2']bipyridinyl-6-yl)pyridazin-3-yl]propene-1-one (10): 3,6-bis-(4-propylsulfanyl-[2,2']bipyridinyl-6-yl)pyridazine (11): NaH (0.544 g 60% w/w in mineral oil, 13.6 mmol) was added to a solution of **9** (3.87 g, 8.0 mmol) and 2-acetylpyridine (1.45 g, 12.0 mmol) in THF/DMSO (freshly distilled THF (100 mL) and dry DMSO (50 mL)). The resulting purple solution was stirred at room temperature under nitrogen overnight after which acetic acid (48 mL) and ammonium acetate (8 g) were added. The mixture was refluxed for 30 min, cooled, slowly poured into ice-cold aqueous sodium hydrogen carbonate, and the product extracted with chloroform. The organic phases were combined, washed with water, dried over sodium sulfate, and the solvent removed on a rotary evaporator. The products were isolated by column chromatography (alumina, chloroform/hexane (80% v/v) eluent). The fractions containing the products were combined and the solvent removed resulting in two products which were washed with acetone to give **10** (0.993 g; 24% yield) as a yellow powder and **11** (0.316 g; 7% yield) as an off-white powder.

10: M.p. 160.0–160.7 °C; R_f (alumina, CH_2Cl_2): 0.74; ^1H NMR (200 MHz, CDCl_3 , 25 °C): δ = 8.81 (d, J = 8.8 Hz, 1H), 8.67 (bd, J = 4.7 Hz, 1H), 8.65 (d, J = 1.7 Hz, 1H), 8.51 (d, J = 7.9 Hz, 1H), 8.39 (d, J = 8.8 Hz, 1H) 8.37 (d, J = 2.6 Hz, 1H), 7.86 (s, 1H), 7.82 (ddd, J = 7.8 Hz, 7.8 Hz, 1.8 Hz, 1H), 7.31 (m, 1H), 3.13 (m, 6H), 1.80 (m, 6H), 1.10 ppm (m, 9H); ^{13}C NMR (50 MHz, CDCl_3 , 25 °C): δ = 181.51, 169.70, 159.06, 157.07, 155.41, 155.36, 152.58, 151.79, 149.21, 136.94, 126.49, 125.73, 124.17, 121.39, 119.06, 118.56, 108.95, 108.90, 36.49, 33.69, 32.96, 22.37, 21.93, 20.86, 13.73, 13.65 ppm; IR (KBr): $\tilde{\nu}$ = 2961, 2926, 2869, 1618, 1578, 1563, 1540, 1475, 1425, 1413, 1387, 1218, 1096, 1075, 981, 859, 796 cm^{-1} ; MS (FAB +): m/z : 511.1 (100%, MH^+); elemental analysis calcd (%) for $\text{C}_{26}\text{H}_{30}\text{N}_4\text{O}_3$ (510.74): C 61.15, H 5.92, N 10.97; found: C 61.14, H 5.80, N 11.02.

11: M.p. 204.2–204.8 °C; R_f (alumina, CH_2Cl_2): 0.58; ^1H NMR (200 MHz, CDCl_3 , 25 °C): δ = 8.84 (s, 2H), 8.71 (bd, J = 4.8 Hz, 2H), 8.65 (d, J = 1.7 Hz, 2H), 8.57 (d, J = 7.9 Hz, 2H), 8.40 (d, J = 1.7 Hz, 2H), 7.87 (ddd, J = 7.8 Hz, J = 7.8 Hz, J = 1.7 Hz, 2H), 7.35 (m, 2H), 3.18 (t, J = 7.3 Hz, 4H), 1.84 (tq, J = 7.3 Hz, 7.3 Hz 4H), 1.13 ppm (t, J = 7.4 Hz, 6H); ^{13}C NMR (50 MHz, CDCl_3 , 25 °C): δ = 158.17, 155.68, 155.20, 152.55, 152.33, 149.28, 136.97, 125.46, 124.10, 121.42, 119.07, 117.89, 32.95, 21.97, 13.70 ppm; IR (KBr): $\tilde{\nu}$ = 2961, 2870, 1576, 1561, 1542, 1449, 1424, 1398, 1379, 1292, 1241, 1094, 988, 851, 823, 792 cm^{-1} ; MS (FAB +): m/z : 537.2 (100%, MH^+); elemental analysis calcd (%) for $\text{C}_{30}\text{H}_{28}\text{N}_6\text{S}_2$ (536.72): C 67.14, H 5.26, N 15.66; found: C 67.20, H 5.34, N 15.87.

6-(6-[6-(1-Ethoxyvinyl)pyridazin-3-yl]-4-propylsulfanylpyridin-2-yl)pyridazin-3-yl)-4-propylsulfanyl-[2,2']bipyridinyl (12): NaH (46 mg 60% w/w in mineral oil, 1.150 mmol) was added to a solution of **10** (391 mg, 0.766 mmol) and **8** (206 mg, 1.072 mmol) in THF/DMSO (freshly distilled THF (15 mL) and dry DMSO (5 mL)). The resulting purple solution was stirred at room temperature under nitrogen overnight after which acetic acid (7 mL) and ammonium acetate (1.5 g) were added. The mixture was refluxed for 30 min, cooled, slowly poured into aqueous sodium hydrogen carbonate, and the product extracted with chloroform. The organic phases were combined, washed with water, and the solvent removed on a rotary evaporator. The product was isolated by column chromatography (alumina, chloroform/hexane (80% v/v) eluent). The fractions containing the product were combined, the solvent removed, and the crude product washed with acetone to give **12** (0.152 g; 33% yield) as an off-white powder. M.p. 153.0–155.6 °C (decomp); R_f (alumina, CH_2Cl_2): 0.53; ^1H NMR (200 MHz, CDCl_3 , 25 °C): δ = 8.82–8.51 (m, 8H), 8.37 (d, J = 1.7 Hz, 1H), 7.94 (d, J = 8.9 Hz, 1H), 7.86 (ddd, J = 7.8 Hz, J = 7.8 Hz, J = 1.7 Hz, 1H), 7.34 (m, 1H), 5.86 (d, J = 2.2 Hz, 1H), 4.56 (d, J = 2.2 Hz, 1H), 4.04 (q, J = 7.0 Hz, 2H) 3.15 (t, J = 7.2, 2H) 3.14 (t, J = 7.2, 2H), 1.82 (tq, J = 7.2 Hz, 7.2 Hz, 4H), 1.48 (t, J = 6.9 Hz, 3H) 1.12 ppm (t, J = 7.4 Hz, 6H); ^{13}C NMR (50 MHz, CDCl_3 , 25 °C): δ = 158.18, 157.77, 157.02, 156.19, 155.86, 155.60, 155.13, 153.08, 152.62, 152.55, 152.37, 152.17, 149.25, 136.93, 125.40, 125.25, 124.75, 124.10, 123.18, 121.38, 119.02, 118.96, 118.75, 117.84, 87.10, 63.81, 32.95, 21.93, 21.86, 14.60, 13.70 ppm; IR (KBr): $\tilde{\nu}$ = 2961, 2929, 2871, 1698, 1577, 1540, 1456, 1414, 1388, 1362, 1263, 1231, 1108, 1096, 1046, 988, 854, 824, 808 cm^{-1} ; MS (FAB +): m/z : 608.0 (100%, MH^+); elemental analysis calcd (%) for

$\text{C}_{33}\text{H}_{33}\text{N}_7\text{O}_2\text{S}_2$ (607.80): C 65.21, H 5.47, N 16.13; found: C 65.28, H 5.44, N 16.32.

1-(6-[4-propylsulfanyl-6-[6-(4-propylsulfanyl-[2,2']bipyridinyl-6-yl)pyridazin-3-yl]pyridazin-2-yl]pyridazin-3-yl)ethanone (13): Compound **12** (0.15 g, 0.247 mmol) was suspended in acetone (9 mL) and 2N HCl (1 mL). The reaction mixture was shaken overnight, the solid collected and washed with aqueous sodium hydrogen carbonate, water, and acetone to give **13** as an off-white product (0.14 g; 97% yield). This product was used in the subsequent reaction as such. An analytically pure sample of **13** was obtained after column chromatography (alumina, chloroform/hexane (80% v/v) eluent). M.p. 202.60–205.9 °C (decomp); R_f (alumina, CH_2Cl_2): 0.56; ^1H NMR (200 MHz, CDCl_3 , 25 °C): δ = 8.66–8.38 (m, 8H), 8.22 (d, J = 1.6 Hz, 1H), 8.18 (d, J = 8.8 Hz, 1H), 7.78 (ddd, J = 7.8 Hz, J = 7.8 Hz, J = 1.7 Hz, 1H), 7.28 (m, 1H), 3.04 (t, J = 7.3 Hz, 4H), 2.92 (s, 3H) 1.84 (tq, J = 7.3 Hz, 7.3 Hz, 4H), 1.09 ppm (t, J = 7.3 Hz, 6H); ^{13}C NMR (50 MHz, CDCl_3 , 25 °C): δ = 198.16, 159.35, 158.03, 157.20, 155.46, 155.34, 154.93, 153.43, 152.47, 151.72, 151.43, 149.17, 136.82, 125.31, 125.23, 125.18, 124.96, 124.03, 121.20, 119.42, 119.26, 118.80, 117.62, 32.95, 32.89, 26.26, 21.85, 21.71, 13.71 ppm; IR (KBr): $\tilde{\nu}$ = 2961, 2929, 2871, 1698, 1577, 1540, 1456, 1414, 1388, 1362, 1263, 1231, 1108, 1096, 1046, 988, 854, 824, 808 cm^{-1} ; MS (FAB +): m/z : 580.2 (100%, MH^+); elemental analysis calcd (%) for $\text{C}_{31}\text{H}_{29}\text{N}_7\text{O}_2\text{S}_2$ (579.74): C 64.23, H 5.04, N 16.91; found: C 64.32, H 4.99, N 17.08.

3,6-Bis-[4-propylsulfanyl-6-(6-[4-propylsulfanyl-6-[6-(4-propylsulfanyl-[2,2']bipyridinyl-6-yl)pyridazin-3-yl]pyridin-2-yl)pyridazin-3-yl)pyridin-2-yl]pyridazine (3): NaH (32 mg 60% w/w in mineral oil, 0.800 mmol) was added to a solution of **13** (350 mg, 0.604 mmol) and **9** (121 mg, 0.250 mmol) in THF/DMSO (freshly distilled THF (30 mL) and dry DMSO (6 mL)). The resulting purple solution was stirred at room temperature under nitrogen overnight after which acetic acid (6.5 mL) and ammonium acetate (2.3 g) were added. The mixture was refluxed for 45 min, cooled, slowly poured into aqueous sodium hydrogen carbonate, and the product extracted with chloroform. The organic phases were combined, washed with water, and the solvent removed on a rotary evaporator. The product was isolated by column chromatography (alumina, dichloromethane eluent). The fractions containing the product were combined, and the solvent was removed to give **3** (71.2 mg; 19% yield) as an off-white powder. M.p. 326.2–329.0 °C (decomp); R_f (alumina, CH_2Cl_2): 0.14; ^1H NMR (500.13 MHz, CDCl_3 (29 mm), 55 °C): δ = 8.17–7.77 (m, 26H), 7.06 (m, 2H), 6.53 (m, 2H), 3.06 (t, 3J = 7.1 Hz, 4H), 3.02 (t, 3J = 7.1 Hz, 4H), 2.98 (t, 3J = 7.1 Hz, 4H), 1.88–1.70 (m, 12H), 1.21 (t, 3J = 7.4 Hz, 6H), 1.17 (t, 3J = 7.4 Hz, 6H), 1.10 ppm (t, 3J = 7.4 Hz, 6H); ^{13}C NMR (125.77 MHz, CDCl_3 (29 mm), 55 °C): δ = 157.08, 156.60, 156.54, 156.53, 156.50, 154.60, 154.09, 153.25, 153.04, 152.16, 151.32, 151.24, 151.16, 151.14, 148.72, 135.72, 123.99, 123.84, 123.79, 123.74, 123.04, 120.14, 118.36, 118.32, 118.15, 118.03, 118.02, 117.36, 33.22, 33.13, 33.00, 21.80, 21.69, 21.68, 13.91, 13.84, 13.65 ppm; IR (KBr): $\tilde{\nu}$ = 2960, 2925, 2870, 1577, 1545, 1458, 1390, 1097, 988, 850, 812 cm^{-1} ; UV/Vis (CH_2Cl_2): λ_{max} (ϵ) = 296 (202000); MS (FAB +): m/z : 1453.5 (100%, $[\text{M}]^+$); elemental analysis calcd (%) for $\text{C}_{78}\text{H}_{72}\text{N}_{18}\text{S}_6$ (1453.92): C 64.44, H 4.99, N 17.34; found: C 64.42, H 5.01, N 17.22.

Acknowledgements

Dr. Roland Graff is thanked for performing the high-field NMR experiments. Olof Ramström's assistance with the dimerization calculations is greatly appreciated. Ulrich Ziener and Ahmed Mourran are thanked for help interpreting the AFM results. L.A.C. thanks the Natural Sciences and Engineering Research Council of Canada (NSERC) and the Centre National de la Recherche Scientifique, France (CNRS) for financial support. J.-C.H. and M.S. acknowledge the financial support of l'Institut National de la Santé et de la Recherche Médicale (INSERM). E.R. thanks the Centre de Supercomputació de Catalunya (CESCA) for the computing resources.

[1] S. H. Gellman, *Acc. Chem. Res.* **1998**, 37, 173–180.

[2] D. J. Hill, M. J. Mio, R. B. Prince, T. S. Hughes, J. S. Moore, *Chem. Rev.* **2001**, 101, 3893–4012.

- [3] K. Kirshenbaum, R. N. Zuckermann, K. A. Dill, *Curr. Opinion Struc. Biol.* **1999**, *9*, 530–535; A. E. Barron, R. N. Zuckermann, *Curr. Opinion Chem. Biol.* **1999**, *3*, 681–687.
- [4] M. S. Cubberley, B. L. Iverson, *Curr. Opin. Chem. Biol.* **2001**, *5*, 650–653.
- [5] H. S. Chan, K. Dill, *Physics Today* **1993**, 232.
- [6] G. S. Hanan, J.-M. Lehn, N. Kyritsakas, J. Fischer, *J. Chem. Soc. Chem. Commun.* **1995**, 765–766.
- [7] G. S. Hanan, U. S. Schubert, D. Volkmer, E. Rivière, J.-M. Lehn, N. Kyritsakas, J. Fischer, *Can. J. Chem.* **1997**, *75*, 169–182.
- [8] D. M. Bassani, J.-M. Lehn, G. Baum, D. Fenske, *Angew. Chem.* **1997**, *109*, 1931–1933; *Angew. Chem. Int. Ed. Engl.* **1997**, *36*, 1845–1847.
- [9] D. M. Bassani, J.-M. Lehn, *Bull. Soc. Chim. Fr.* **1997**, *134*, 897–906.
- [10] M. Ohkita, J.-M. Lehn, G. Baum, D. Fenske, *Chem. Eur. J.* **1999**, *5*, 3471–3481.
- [11] M. Ohkita, J.-M. Lehn, G. Baum, D. Fenske, *Heterocycles* **2000**, *52*, 103–109.
- [12] L. A. Cuccia, J.-M. Lehn, J.-C. Homo, M. Schmutz, *Angew. Chem.* **2000**, *112*, 239–243; *Angew. Chem. Int. Ed.* **2000**, *39*, 233–237.
- [13] A. Petitjean, L. A. Cuccia, J.-M. Lehn, H. Nierengarten, M. Schmutz, *Angew. Chem.* **2002**, *114*, 1243–1246; *Angew. Chem. Int. Ed.* **2002**, *41*, 1195–1198.
- [14] K. M. Gardinier, R. G. Khoury, J.-M. Lehn, *Chem. Eur. J.* **2000**, *6*, 4124–4131.
- [15] V. Berl, I. Huc, R. G. Khoury, M. J. Krische, J.-M. Lehn, *Nature* **2000**, *407*, 720–723.
- [16] V. Berl, I. Huc, R. G. Khoury, J.-M. Lehn, *Chem. Eur. J.* **2001**, *7*, 2798–2809.
- [17] V. Berl, I. Huc, R. G. Khoury, J.-M. Lehn, *Chem. Eur. J.* **2001**, *7*, 2810–2820.
- [18] Y. Hamuro, S. J. Geib, A. D. Hamilton, *Angew. Chem.* **1994**, *106*, 465–467; *Angew. Chem. Int. Ed. Engl.* **1994**, *33*, 446–448.
- [19] Y. Hamuro, S. J. Geib, A. D. Hamilton, *J. Am. Chem. Soc.* **1996**, *118*, 7529–7541.
- [20] Y. Hamuro, S. J. Geib, A. D. Hamilton, *J. Am. Chem. Soc.* **1997**, *119*, 10587–10593.
- [21] J. Zhu, R. D. Parra, H. Zeng, E. Skrzypczak-Jankun, X. C. Zeng, B. Gong, *J. Am. Chem. Soc.* **2000**, *122*, 4919–4220.
- [22] B. Gong, *Chem. Eur. J.* **2001**, *7*, 4336–4342.
- [23] K. Burgess, K. S. Linthicum, H. Shin, *Angew. Chem.* **1995**, *107*, 975–977; *Angew. Chem. Int. Ed. Engl.* **1995**, *34*, 907–909.
- [24] J. C. Nelson, J. G. Saven, J. S. Moore, P. G. Wolynes, *Science* **1997**, *277*, 1793–1796.
- [25] P. S. Corbin, S. C. Zimmerman, P. A. Thiessen, N. A. Hawryluk, T. J. Murray, *J. Am. Chem. Soc.* **2001**, *123*, 10475–10488.
- [26] S. T. Howard, *J. Am. Chem. Soc.* **1996**, *118*, 10269–10274; A. Göller, U.-W. Grummt, *Chem. Phys. Lett.* **2000**, *321*, 399–405.
- [27] J. P. Glusker, in *The Crystal as a Supramolecular Entity*, Vol. 2 (Ed.: G. R. Desiraju), Wiley, Chichester, **1996**, pp. 235–309.
- [28] F. R. Heitzler, M. Neuburger, M. Zehnder, E. C. Constable, *Liebigs Ann./Recueil* **1997**, 297–301.
- [29] A. Aggeli, I. A. Nyrkova, M. Bell, R. Harding, L. Carrick, T. C. B. McLeish, A. N. Semenov, N. Boden, *Proc. Natl. Acad. Sci. USA* **2001**, *98*, 11857–11862.
- [30] K. T. Potts, *Bull. Soc. Chim. Belg.* **1990**, *99*, 741–768; K. T. Potts, K. A. Gheysen Raiford, M. Keshavarz-K, *J. Am. Chem. Soc.* **1993**, *115*, 2793–2807–2807.
- [31] R. E. Reid, P. L. Franchini in *Peptide and Protein Drug Analysis* (Ed.: R. E. Reid), Marcel Dekker, New York, **2000**, pp. 1–80.
- [32] R. Gompper, H.-J. Mair, K. Polborn, *Synthesis* **1997**, 696–718.
- [33] R. H. Martin, N. Defay, H. P. Figeys, M. Flammang-Barbieux, J. P. Cosyn, M. Gelbcke, J. J. Schurter, *Tetrahedron* **1969**, *25*, 4985–4998.
- [34] H. Wynberg, *Acc. Chem. Res.* **1971**, *4*, 65–73.
- [35] A. S. Shetty, J. Zhang, J. S. Moore, *J. Am. Chem. Soc.* **1996**, *118*, 1019–1027.
- [36] T. J. Katz, *Angew. Chem.* **2000**, *112*, 1997–1999; *Angew. Chem. Int. Ed.* **2000**, *39*, 1921–1923.
- [37] D. J. Prockop, *Matrix Biology* **1998**, *16*, 519–528.
- [38] D. J. Prockop, A. Fertala, *J. Struct. Biol.* **1998**, *122*, 111–118.
- [39] C. Ionescu-Zanetti, R. Khurana, J. R. Gillespie, J. S. Petrick, L. C. Trabachino, L. J. Minert, S. A. Carter, A. L. Fink, *Proc. Natl. Acad. Sci. USA* **1999**, *96*, 13175–13179.
- [40] J.-C. Rochet, P. T. Lansbury Jr., *Curr. Opin. Structural Biol.* **2000**, *10*, 60–68.
- [41] G. P. Saborio, B. Permann, C. Soto, *Nature* **2001**, *411*, 810–813.
- [42] K. P. McGrath, M. M. Butler in *Protein-Based Materials* (Eds.: K. McGrath, D. Kaplan), Birkhauser, Boston, **1997**, pp. 251–279.
- [43] H. Engelkamp, S. Middelbeek, R. J. M. Nolte, *Science* **1999**, *284*, 785–788.
- [44] A. S. Shetty, P. R. Fischer, K. F. Stork, P. W. Bohn, J. S. Moore, *J. Am. Chem. Soc.* **1996**, *118*, 9409–9414.
- [45] O. Y. Mindyuk, P. A. Heiney, *Adv. Mater.* **1999**, *11*, 341–344.
- [46] E. J. Osburn, L.-K. Chau, S.-Y. Chen, N. Collins, D. F. O'Brien, N. R. Armstrong, *Langmuir* **1996**, *12*, 4784–4796.
- [47] P. E. Smolenyak, E. J. Osburn, S.-Y. Chen, L.-K. Chau, D. F. O'Brien, N. R. Armstrong, *Langmuir* **1997**, *13*, 6568–6576.
- [48] P. Smolenyak, R. Peterson, K. Nebesny, M. Törker, D. F. O'Brien, N. R. Armstrong, *J. Am. Chem. Soc.* **1999**, *121*, 8628–8636.
- [49] J. A. Soderquist, G. J.-H. Hsu, *Organometallics* **1982**, *1*, 830–833.

Received: February 25, 2002 [F3899]